B. Erdmann   J. Lang   S. Matera   K. Wilmański

Adaptive Linearly Implicit Methods for Linear Poroelastic Equations

Adaptive Linearly Implicit Methods for Linear Poroelastic Equations

Bodo Erdmann[1] Jens Lang[2] Sebastian Matera[1]
Krzysztof Wilmański[3]

Abstract

Adaptive numerical methods in time and space are introduced and studied for linear poroelastic models in two and three space dimensions.

We present equivalent models for linear poroelasticity and choose both the *displacement-pressure* and the *stress-pressure* formulation for our computations. Their discretizations are provided by means of linearly implicit schemes in time and linear finite elements in space. Our concept of adaptivity opens a way to a fast and reliable simulation of different loading cases defined by corresponding boundary conditions.

We present some examples using our code Kardos and show that the method works efficiently. In particular, it could be used in the simulation of some bone healing models.

Keywords: Poroelasticity, Biot's model, bone healing, adaptive finite elements, adaptive time integration, Rosenbrock methods

1 Introduction

A lot of phenomena in nature can be modelled by poroelastic equations. An important example is the extraction of oil from its deposit. The context where this study has been motivated is the initial phase of bone healing. Here the movement of the fluid in the soft tissue filling the fracture gap is assumed to influence the generation of new bone tissue.

---

[1]Zuse Institute Berlin
[2]Technische Universität Darmstadt
[3]Technische Universität Berlin

Goal of our work is to develop a numerical code which provides solutions adaptively in time and in space. This might open a way to fast and reliable simulation of different loading cases defined by corresponding boundary conditions.

In the next section we present two equivalent models for linear poroelasticity as they are presented in WANG [41]. These models yield the same results as the classical equations introduced by BIOT [6]. In particular, we use a *displacement-pressure* and a *stress-pressure* formulation. The same models are derived by WILMAŃSKI [44]. His formulation is the result of a linearization in a more general, nonlinear theory derived with help of the theory of mixtures [43].

In Section 3 we describe the discretization of the poroelastic equations in detail and introduce our numerical code Kardos. A review of other discretization methods is given by LIPNIKOV [31]. We refer also to recent work of CUI ET AL. [13], CHEN ET AL. [9], GASPAR ET. AL. [22], EWING ET AL. [21], and literature cited therein. Our algorithm is based on linearly-implicit Rosenbrock methods for time discretization and linear finite elements in space, as it is used by LANG [28] in tradition of a long-time research at ZIB, see BORNEMANN [7], DEUFLHARD, LANG, and NOWAK [17], DEUFLHARD, LEINEN and YSERENTANT [18], BORNEMANN, ERDMANN, and KORNHUBER [8]. It comprises adaptive control of the time steps as well as the adaption of the spatial meshes which has proven in many applications to be an advantage of this method. This ansatz is justified by our restriction to the variables *displacement*, *pressure*, and *stress*. It may find its limitation if also the velocity of the fluid has to be computed. In the latter case mixed finite element methods should be more advantageous.

In Section 4, we present some examples showing that the method works efficiently and that it can be used in the simulation of geological problems as well as for some bone healing models. However, there are also some (extreme) samples of problem parameters leading to a bad performance of the iterative solver for the inherent linear algebraic systems in each time step.

2   Biot's model for linear poroelasticity

A general introduction into the theory of mixtures is given by TRUESDELL [38] and the application to poroelastic materials by WILMAŃSKI [42, 45]. Porous media with mass exchange need an extended set of basic fields. Such systems have been studied for example in ALBERS [3] and MATERA [33]. For a detailed review of the classical theory of linear poroelasticity as for the first time given by BIOT [6] we refer to WANG [41] and COUSSY [10].

In this paper, we follow the presentation of WANG [41] based on the following assumptions:

- the temperature of the material is constant,

- there is no mass exchange between the solid phase and fluid phase,

- the fluid behaves macroscopically as an ideal fluid,

- only small deformations occur.

We use the following notation:

$u^s = (u_1^s, u_2^s, u_3^s)$ displacement vector of the solid

$v^s = (v_1^s, v_2^s, v_3^s)$ velocity vector of the solid

$v^f = (v_1^f, v_2^f, v_3^f)$ velocity vector of the fluid

$T = (\sigma_{ij})_{i,j=1,2,3}$ total stress tensor

$tr\, T = \sigma_{11} + \sigma_{22} + \sigma_{33}$ trace of stress tensor T
p pore fluid pressure

δ_{ij} Kronecker delta

A set of representative material parameters is assembled in Table 1.

G	shear modulus of the poroelastic medium under the drained condition
E	Young's modulus
ν	drained Poisson's ratio
ν_u	undrained Poisson's ratio
ϕ	porosity
B	Skempton's coefficient
K	bulk modulus of the poroelastic medium under the drained condition
K_f	fluid bulk modulus
k	permeability
μ	fluid viscosity
η	poroelastic stress coefficient
α	Biot-Willis coefficient

Table 1: Parameters chosen in linear poroelastic models

We have the following relationships between these parameters.

$$G = \frac{E}{2(1+\nu)} \qquad K = \frac{E}{3(1-2\nu)}$$

$$\eta = \frac{1-2\nu}{2(1-\nu)}\alpha \qquad B = \frac{3(\nu_u - \nu)}{\alpha(1+\nu_u)(1-2\nu)}$$

The formulation we choose to serve as starting point for our considerations is a linearization of the general nonlinear balance equations with respect to the deformation. Thus the presented theory is only valid for small deformations of the solid. A detailed representation of the results of the linearized mixture theory can be found in [44] and [45].

Furthermore, an influence of relative accelerations is neglected in our model. Then the constitutive relations for the total stress and the pore pressure read as follows.

(u, p)-formulation

DPF:
$$-G\,\nabla^2\,u_i^s - \frac{G}{1-2\nu}\,\frac{\partial}{\partial x_i}\sum_{k=1}^{3}\frac{\partial u_k^s}{\partial x_k} + \alpha\,\frac{\partial p}{\partial x_i} = 0, \qquad i = 1,2,3 \qquad (1)$$

$$\frac{\alpha(1-\alpha B)}{KB}\,\frac{\partial p}{\partial t} + \alpha\,\frac{\partial\,(\nabla\cdot u^s)}{\partial t} - \frac{k}{\mu}\,\nabla^2\,p = 0 \qquad (2)$$

This can be considered as the *displacement-pressure* formulation of linear poroelasticity (DPF).

(σ, p)-formulation

Based on the geometric compatibility conditions for the components of the solid's strain tensor and the momentum balance $\nabla \cdot T = 0$ we can derive equations only with the components of the stress tensor and the pressure as unknown fields, which can be written in the form of (3), compare COWIN [12].

BMF:
$$-\nabla^2\,\sigma_{ij} - \frac{1}{1+\nu}\,\frac{\partial^2}{\partial x_i \partial x_j}\sum_{k=1}^{3}\sigma_{kk} + 2\eta\left[\frac{1-\nu}{1+\nu}\,\frac{\partial^2 p}{\partial x_i \partial x_j} + \delta_{ij}\,\nabla^2 p\right] = 0 \quad (3)$$

$$\frac{\alpha}{KB}\left[\frac{B}{3}\frac{\partial}{\partial t}\sum_{k=1}^{3}\sigma_{kk} + \frac{\partial p}{\partial t}\right] - \frac{k}{\mu}\nabla^2\,p = 0 \qquad (4)$$

4

This *stress-pressure* formulation (BMF) is also well-known as the BELTRAMI-MICHELL model for poroelastic media.

The system (3) of 6 equations leads by some elementary rearrangement to the following scalar equation (5) for the trace of the stress tensor.

SBMF:
$$\nabla^2 \left[\operatorname{tr} T + 4\eta p \right] = 0 \tag{5}$$

$$\frac{\alpha}{KB} \left[\frac{B}{3} \frac{\partial \operatorname{tr} T}{\partial t} + \frac{\partial p}{\partial t} \right] - \frac{k}{\mu} \nabla^2 p = 0 \tag{6}$$

The equations (5) and (6) can now be used to calculate the unknown quantities $\operatorname{tr} T$ and p. They will be called *simplified* BELTRAMI-MICHELL formulation (SBMF). It is useful if one is not interested in all the components of the stress tensor . Otherwise one has to use (1) or (3) instead of (5). Using the DPF it is possible to calculate the stress tensor from the values of the displacement field.

We remark that the parabolic equations (2), (4), and (6) are related to DARCY's law which describes the relationship between p and v^f:

$$v := v^f - v^s = -\frac{k}{n_0 \mu} \nabla p \tag{7}$$

Boundary conditions

Natural boundary conditions are normally derived from jump conditions on singular walls using the (global) balances of mass, momentum etc.. For example, boundary conditions are discussed in ALBERS [3]. For the BMF it is hard to find boundary conditions, because the compatibility conditions can not be derived from global balances. To provide boundary conditions for the stress components which fulfill the momentum balance div $T = 0$ is a problem for itself, compare corresponding considerations of PATNAIK, HOPKINS [34] for linear elastic problems. Due to this lack of a "complete BELTRAMI-MICHELL" formulation for poroelasticity we only use Dirichlet boundary conditions for the stress components in our examples.

Considering jump conditions makes only sense if one knows the production of the considered quantity on the wall. The partial momenta are of no use since we do not know the effect of friction at the singular wall without any further information. Other boundary conditions are microscopically motivated or empirical. In the following we will require the velocity of the solid and the velocity of the boundary to be the same.
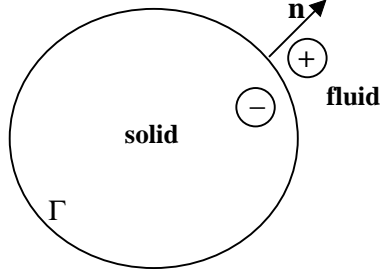
Figure 1: Boundary between solid and fluid in a porous medium.

Conservation of fluid's mass: We assume vanishing mass sources in the porous media and the same we require for the boundary. Thus the fluid's mass is a conserved quantity. This leads to the jump condition of the mass flux

$$\rho^{f-}(v^{f-} - v^s) \cdot n \quad = \quad \rho^{f+}(v^{f+} - v^s) \cdot n$$

where $v^s \cdot n$ is the velocity of the boundary identified with the velocity of the skeleton.

Conservation of the total momentum: The conservation of the total momentum leads to the jump conditions for the total stress (in the linearized model)

$$(T^+)\, n - (T^-)\, n = 0.$$

For $T^- = -p_{ext}I$, $T^+ = T$ (in porous medium) we get the boundary condition

$$T\, n + p_{ext}\, n = 0.$$

Normal mass flux: For the normal mass flux we have the DERESIEWICZ condition

$$\rho^{f-}(v^{f-} - v^s) \cdot n = \alpha_D n_0 (p - p_{ext})$$

with surface permeability α_D. Applying DARCY's law (7) this reads as

$$-\rho^{f-}\frac{k}{n_0 \mu}\nabla p \cdot n = \alpha_D n_0 (p - p_{ext})$$

There are two important special cases

$$
\begin{array}{lll}
\alpha_D \longrightarrow 0 & - & \text{impermeable boundary} \\
\alpha_D \longrightarrow \infty & - & \text{ideal permeable boundary, i.e., } p = p_{ext}.
\end{array}
$$

3   Numerical Discretization

Each of the linear poroelastic models DPF, BMF, or SBMF is discretized by linearly implicit methods in time and adaptive finite elements in space, using the Kardos library [20, 2].

One of the important requirements that modern software has to meet is to judge the quality of its numerical approximations in order to assess safely the modelling process. Adaptive methods provide a posteriori error estimates and appropriate strategies to improve the accuracy. They are now implemented in real-life applications and becoming a standard feature in simulation programs. The present paper reports on one successful way to construct discretization methods adaptive in space and time which are applicable to a wide range of practically relevant problems.

The three quasi-stationary formulations DPF, BMF, and SBMF fit into the scheme of reaction-diffusion problems of the form

$$B(x,t,u,\operatorname{grad} u)\partial_t u = \operatorname{div}\left(D(x,t,u,\operatorname{grad} u)\operatorname{grad} u\right) + F(x,t,u,\operatorname{grad} u) \quad (8)$$

with suitable boundary and initial conditions. The vector-valued solution $u = (u_1, \ldots, u_m)^T$ is supposed to be unique.

In the classical method of lines (MOL) approach, the spatial discretization is done once and kept fixed during the time integration. Here, we allow a local spatial refinement in each time step, which results in a discretization sequence first in time then in space. The spatial discretization is considered as a perturbation, which has to be controlled within each time step. Combined with a posteriori error estimates this approach is known as adaptive Rothe method. First theoretical investigations have been made by BORNEMANN [7] for linear parabolic equations. LANG and WALTER [30] have generalized the adaptive Rothe approach to reaction-diffusion systems. A rigorous analysis for nonlinear parabolic systems is given in LANG [28]. For a comparative study, we refer to DEUFLHARD, LANG, and NOWAK [17].

Since differential operators give rise to infinite stiffness, often an implicit method is applied to discretize in time. We use linearly implicit methods of Rosenbrock type, which are constructed by incorporating the Jacobian directly into the formula. These methods offer several advantages. They completely avoid the solution of nonlinear equations, that means no Newton iteration has to be controlled. There is no problem to construct Rosenbrock methods with optimum linear stability properties for stiff equations. According to their one-step nature, they allow a rapid change of step sizes and an efficient adaptation of the spatial discretization in each time step. Moreover, a simple embedding technique can be used to estimate the error in time satis-

factorily. A description of the main idea of linearly implicit methods is given in Subsection 3.1.

Linear finite elements are used for the spatial discretization. To estimate the error in space, the hierarchical basis technique has been extended to Rosenbrock schemes in LANG [28]. Hierarchical error estimators have been accepted to provide efficient and reliable assessment of spatial errors. They can be used to steer a multilevel process, which aims at getting a successively improved spatial discretization drastically reducing the size of the arising linear algebraic systems with respect to a prescribed tolerance (BORNEMANN, ERDMANN, and KORNHUBER [8], DEUFLHARD, LEINEN and YSERENTANT [18], BANK and SMITH [5]). A brief introduction to multilevel finite element methods is given in Subsection 3.2.

The described algorithm has been coded in the fully adaptive software package Kardos at the Konrad-Zuse-Zentrum in Berlin. Several types of embedded Rosenbrock solvers and adaptive finite elements were implemented. Kardos is based on the Kaskade-toolbox [19]. Nowadays both codes are efficient and reliable workhorses to solve a wide class of PDEs in one, two, or three space dimensions.

3.1 Linearly implicit methods

In this section a short description of the linearly implicit discretization idea is given. For ease of presentation, we firstly set $B = I$ in (8) and consider the autonomous case. Then we can look at (8) as an abstract Cauchy problem of the form

$$\partial_t u = f(u) , \quad u(t_0) = u_0 , \quad t > t_0 , \tag{9}$$

where the differential operators and the boundary conditions are incorporated into the nonlinear function $f(u)$. Since differential operators give rise to infinite stiffness, often an implicit discretization method is applied to integrate in time. The simplest scheme is the implicit (backward) Euler method

$$u_{n+1} = u_n + \tau \, f(u_{n+1}) , \tag{10}$$

where $\tau = t_{n+1} - t_n$ is the step size and u_n denotes an approximation of $u(t)$ at $t = t_n$. This equation is implicit in u_{n+1} and thus usually a Newton-like iteration method has to be used to approximate the numerical solution itself. The implementation of an efficient nonlinear solver is the main problem for a fully implicit method.

Investigating the convergence of Newton's method in function space, DEU-FLHARD [16] pointed out that one calculation of the Jacobian or an approximation of it per time step is sufficient to integrate stiff problems efficiently.

Using u_n as an initial iterate in a Newton method applied to (10), we find

$$(I - \tau J_n) K_n = \tau f(u_n) , \tag{11}$$

$$u_{n+1} = u_n + K_n , \tag{12}$$

where J_n stands for the Jacobian matrix $\partial_u f(u_n)$. The arising scheme is known as the *linearly implicit* Euler method. The numerical solution is now effectively computed by solving the system of linear equations that defines the increment K_n. Among the methods which are capable of integrating stiff equations efficiently, the linearly implicit methods are the easiest to program, since they completely avoid the numerical solution of nonlinear systems.

A generalization of the linearly implicit approach we will follow here leads to Rosenbrock methods (ROSENBROCK [35]). They have found wide-spread use in the ODE context. Applied to (9) a so-called s-stage Rosenbrock method has the recursive form

$$(I - \tau\gamma_{ii} J_n) K_{ni} = \tau f(u_n + \sum_{j=1}^{i-1} \alpha_{ij} K_{nj}) + \tau J_n \sum_{j=1}^{i-1} \gamma_{ij} K_{nj} , \ i = 1(1)s , \tag{13}$$

$$u_{n+1} = u_n + \sum_{i=1}^{s} b_i K_{ni} , \tag{14}$$

where the step number s and the defining formula coefficients b_i, α_{ij}, and γ_{ij} are chosen to obtain a desired order of consistency and good stability properties for stiff equations (see e.g., HAIRER and WANNER [25], IV.7). We assume $\gamma_{ii} = \gamma > 0$ for all i, which is the standard simplification to derive Rosenbrock methods with one and the same operator on the left-hand side of (13). The linearly implicit Euler method mentioned above is recovered for $s = 1$ and $\gamma = 1$.

For the general system

$$B(t, u)\partial_t u = f(t, u) , \quad u(t_0) = u_0 , \quad t > t_0 , \tag{15}$$

an efficient implementation that avoids matrix-vector multiplications with the Jacobian was given by LUBICH and ROCHE [32]. In the case of a time- or solution-dependent matrix B, an approximation of $\partial_t u$ has to be taken into account, leading to the generalized Rosenbrock method of the form

$$\left(\frac{1}{\tau\gamma} B(t_n, u_n) - J_n\right) U_{ni} = f(t_i, U_i) - B(t_n, u_n) \sum_{j=1}^{i-1} \frac{c_{ij}}{\tau} U_{nj} + \tau\gamma_i C_n$$

$$+ \left(B(t_n, u_n) - B(t_i, U_i)\right) Z_i , \quad i = 1(1)s , \tag{16}$$

where the internal values are given by

$$t_i = t_n + \alpha_i \tau, \quad U_i = u_n + \sum_{j=1}^{i-1} a_{ij} U_{nj}, \quad Z_i = (1 - \sigma_i) z_n + \sum_{j=1}^{i-1} \frac{s_{ij}}{\tau} U_{nj},$$

and the Jacobians are defined by

$$\begin{aligned} J_n &:= \partial_u (f(t, u) - B(t, u)z)_{|u=u_n, t=t_n, z=z_n}, \\ C_n &:= \partial_t (f(t, u) - B(t, u)z)_{|u=u_n, t=t_n, z=z_n}. \end{aligned}$$

This yields the new solution

$$u_{n+1} = u_n + \sum_{i=1}^{s} m_i U_{ni}$$

and an approximation of the temporal derivative $\partial_t u$

$$z_{n+1} = z_n + \sum_{i=1}^{s} m_i \left(\frac{1}{\tau} \sum_{j=1}^{i} (c_{ij} - s_{ij}) U_{nj} + (\sigma_i - 1) z_n \right).$$

The new coefficients can be derived from α_{ij}, γ_{ij}, and b_i [32]. In the special case $B(t, u) = I$, we get (13) setting $U_{ni} = \tau \sum_{j=1,\ldots,i} \gamma_{ij} K_{nj}$, $i = 1, \ldots, s$. Various Rosenbrock solvers have been constructed to integrate systems of the form (15). An important fact is that the formulation (15) includes problems of higher differential index. Thus, the coefficients of the Rosenbrock methods have to be specially designed to obtain a certain order of convergence. Otherwise, order reduction might happen. Among the Rosenbrock methods suitable for index 1 problems we mention ROS2 [15], ROS2POS[40], ROS3P [29], and RODAS4 [25]. More information can be found in [28]. These solvers are appropriate for our simulations in the *displacement-pressure* formulation (1), (2).
Usually, one wishes to adapt the step size in order to control the temporal error. For linearly implicit methods of Rosenbrock type a second solution of inferior order, say $\hat{p}$, can be computed by a so-called embedded formula

$$\begin{aligned} \hat{u}_{n+1} &= u_n + \sum_{i=1}^{s} \hat{m}_i U_{ni}, \\ \hat{z}_{n+1} &= z_n + \sum_{i=1}^{s} \hat{m}_i \left(\frac{1}{\tau} \sum_{j=1}^{i} (c_{ij} - s_{ij}) U_{nj} + (\sigma_i - 1) z_n \right), \end{aligned}$$

where the original weights m_i are simply replaced by $\hat{m}_i$. If p is the order of u_{n+1}, we call such a pair of formulas to be of order $p(\hat{p})$. Introducing an appropriate scaled norm $\|\cdot\|$, the local error estimator

$$r_{n+1} = \|u_{n+1} - \hat{u}_{n+1}\| + \|\tau(z_{n+1} - \hat{z}_{n+1})\| \qquad (17)$$

can be used to propose a new time step by

$$\tau_{n+1} = \frac{\tau_n}{\tau_{n-1}} \left(\frac{TOL_t \, r_n}{r_{n+1} \, r_{n+1}} \right)^{1/(\hat{p}+1)} \tau_n \,. \qquad (18)$$

Here, TOL_t is a desired tolerance prescribed by the user. This formula is related to a discrete PI-controller first established in the pioneering works of GUSTAFSSON, LUNDH, and SÖDERLIND [24, 23].

Rosenbrock methods offer several structural advantages. They preserve conservation properties like fully implicit methods. There is no problem to construct Rosenbrock methods with optimum linear stability properties for stiff equations. Because of their one-step nature, they allow a rapid change of step sizes and an efficient adaptation of the underlying spatial discretizations as will be seen in the next section. Thus, they are attractive for solving real world problems.

3.2   Multilevel finite elements

In the context of PDEs, system (16) consists of linear elliptic boundary value problems. In the spirit of spatial adaptivity a multilevel finite element method is used to solve this system. The main idea of the multilevel technique consists of replacing the solution space by a sequence of discrete spaces with successively increasing dimension to improve their approximation property. A posteriori error estimates provide the appropriate framework to determine where a mesh refinement is necessary and where degrees of freedom are no longer needed. Adaptive multilevel methods have proven to be a useful tool for drastically reducing the size of the arising linear algebraic systems and to achieve high and controlled accuracy of the spatial discretization (see e.g., BANK [4], DEUFLHARD, LEINEN, and YSERENTANT [18], LANG [27]). Let T_h be an admissible finite element mesh at $t = t_n$ and S_h^q be the associated finite dimensional space consisting of all continuous functions which are polynomials of order q on each finite element $T \in T_h$. Then the standard Galerkin finite element approximation $U_{ni}^h \in S_h^q$ of the intermediate values U_{ni} satisfies the equation

$$(L_n \, U_{ni}^h, \phi) = (r_{ni}, \phi) \quad \text{for all } \phi \in S_h^q, \qquad (19)$$

where L_n is the weak representation of the differential operator on the left-hand side in (16) and r_{ni} stands for the entire right-hand side in (16). Since the operator L_n is independent of i its calculation is required only once within each time step.

The linear systems are solved by direct or iterative methods. While direct methods work quite satisfactorily in one-dimensional and even two-dimensional applications, iterative solvers such as Krylov subspace methods perform considerably better with respect to CPU-time and memory requirements for large two- and three-dimensional problems. We mainly use the BICGSTAB- [39] or the GMRES-algorithm [36] with ILU-preconditioning as iterative solver and the library UmfPack Version 4.4 [14] for direct solution. After computing the approximate intermediate values U_{ni}^h a posteriori error estimates can be used to give specific assessment of the error distribution. Considering a hierarchical decomposition

$$S_h^{q+1} = S_h^q \oplus Z_h^{q+1}, \tag{20}$$

where Z_h^{q+1} is the subspace that corresponds to the span of all additional basis functions needed to extend the space S_h^q to higher order, an attractive idea of an efficient error estimation is to bound the spatial error by evaluating its components in the space Z_h^{q+1} only. This technique is known as hierarchical error estimation and has been accepted to provide efficient and reliable assessment of spatial errors (BORNEMANN, ERDMANN, and KORNHUBER [8], DEUFLHARD, LEINEN and YSERENTANT [18], BANK and SMITH [5]). In LANG [28], the hierarchical basis technique has been carried over to time-dependent nonlinear problems. Defining an a posteriori error estimator $E_{n+1}^h \in Z_h^{q+1}$ by

$$E_{n+1}^h = E_{n0}^h + \sum_{i=1}^s m_i E_{ni}^h \tag{21}$$

with E_{n0}^h approximating the projection error of the initial value u_n in Z_h^{q+1} and E_{ni}^h estimating the spatial error of the intermediate value U_{ni}^h, the local spatial error for a finite element $T \in T_h$ can be estimated by $\eta_T := \|E_{n+1}^h\|_T$. The error estimator E_{n+1}^h is computed by linear systems which can be derived from (19). For practical computations the spatially global calculation of E_{n+1}^h is normally approximated by a small element-by-element calculation. This leads to an efficient algorithm for computing a posteriori error estimates which can be used to determine an adaptive strategy to improve the accuracy of the numerical approximation where needed. A rigorous a posteriori error analysis for a Rosenbrock-Galerkin finite element method applied to nonlinear parabolic systems is given in LANG [28]. In our applications we

utilize linear finite elements and measure the spatial errors in the space of quadratic functions.

In order to produce a nearly optimal mesh, those finite elements T having an error η_T larger than a certain threshold are refined. After the refinement improved finite element solutions U_{ni}^h defined by (19) are computed. The whole procedure solve–estimate–refine is applied several times until a prescribed spatial tolerance $\|E_{n+1}^h\| \leq TOL_x$ is reached. To maintain the nesting property of the finite element subspaces coarsening takes place only after an accepted time step before starting the multilevel process at a new time.

4   Applications

Our numerical experiments are focused on solving the *displacement-pressure* formulation (DPF) based on the equations (1), (2) and the simplified *stress-pressure* formulation (SBMF) based on (5), (6). As an alternative we introduced the *stress-pressure* formulation (BMF) using six equations (3) for the components of the stress tensor instead of (5). The BMF is expected to show the same numerical behavior as the SBMF.

We investigate whether our algorithm works for different loading cases for both soft and stiff matter, e.g., charcoal granite or physiological tissues like cortical bone and granulation tissue.

Table 2 shows the values of the parameters for those materials we study in the following examples, compare [41], [11], or [26].

	charcoal granite	bone tissue	granulation tissue
G [Pa]	$19.0 \cdot 10^9$	$5.0 \cdot 10^9$	$0.86 \cdot 10^5$
E [Pa]	$48.3 \cdot 10^9$	$13.2 \cdot 10^9$	$2.00 \cdot 10^5$
ν	0.27	0.32	0.167
ν_u	0.30	0.33	0.5
ϕ	0.02	0.05	0.80
B	0.55	0.40	1.0
K [Pa]	$35.0 \cdot 10^9$	$12.0 \cdot 10^9$	$1.0 \cdot 10^5$
k [m^2]	$1 \cdot 10^{-19}$	$1.5 \cdot 10^{-20}$	$1 \cdot 10^{-17}$
μ	0.001	0.001	0.001
α	0.27	0.14	1.0

Table 2: Poroelastic parameters for some materials

Due to the term *div u* in equation (2) the DPF has first to be modified in order to match the shape of system (8) which we can treat in our code Kardos.

This is done by introducing a new variable h fulfilling the equation $h = \text{div } u$. We choose the Rosenbrock method ROS3P for time discretization. It is of discretization order 3 also in case of time-dependent boundary conditions. Compared to other schemes, e.g., ROS2 or RODAS4, it proved to be the most efficient time integrator in this context. Estimation of the error in time leads to continuously increasing time steps in all the examples. This makes the method more efficient than one based on constant time steps. However, we note that the choice of larger time steps is not surprising because the small values of the permeability k diminish the influence of the diffusion terms in equation (2) or (4). Hence, the lack of further reaction terms let expect that there is only small dynamics in time. With other words: the control of time steps is not the important mean for efficiency in these examples. But possibly for other materials.

The discretization in space is always started on an initial mesh as coarse as possible but fine enough to resolve the characteristics of the particular geometry. All the computations are done for local error tolerances $TOL_t = 0.001$ in time and $TOL_x = 0.001$ in space. Furthermore, due to restriction in the memory of our machine, we request for the problem in three space dimensions (3D) in each time step that the adaptive grid refinement stops when the number of nodes exceeds 100,000. This results in local refinement of depth not less than 3, i.e., at least one of the tetrahedra in the coarse grid is refined 3 times. Assuming that this provides the same accuracy as an corresponding uniform mesh it gets clear that adaptivity may have an eminent advantage for problems with local dynamics. In this report we abstain from investigating this assumption in detail, but refer to the book of LANG [28].
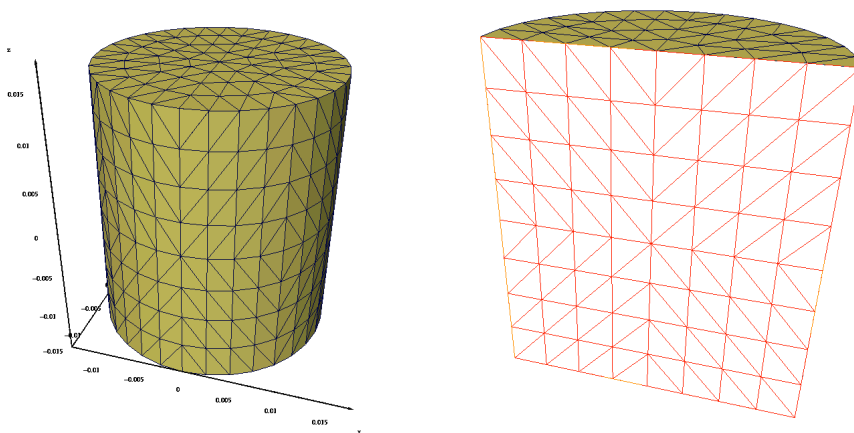

Figure 2: Initial tetrahedral mesh of a cylindrical body.

14

Sometimes the requested accuracy in space is not achieved due to the restriction of the maximum number of nodes in the mesh. Nevertheless the method terminates successfully in all examples with estimated errors close to the requested tolerances.

As an example we present some simulations of loading cases of a cylindrical body.

We use the DPF and the SBMF applying increasing displacement of the top face resp. increasing stress on top and bottom face. In the DPF, the top face is pressed 0.0001 [m] for stiff or 0.001 [m] for soft material uniformly over one second towards the bottom face which is fixed. These two faces are impermeable for the fluid, thus $(v^s - v^f) \cdot n = 0$ holds. At the lateral faces we have for the stress tensor $T^s n = 0$ and for pore pressure $p = 0$ (i.e., the body is drained).

The extent of the body (height: 0.03 m, radius: 0.013 m) and the initial grid for the multilevel algorithm is shown in Figure 2.

4.1 Charcoal granite

First, we want to compare both formulations SBMF and DPF for charcoal granite as an example for stiff tissue. The material parameters and the loading cases are defined above.
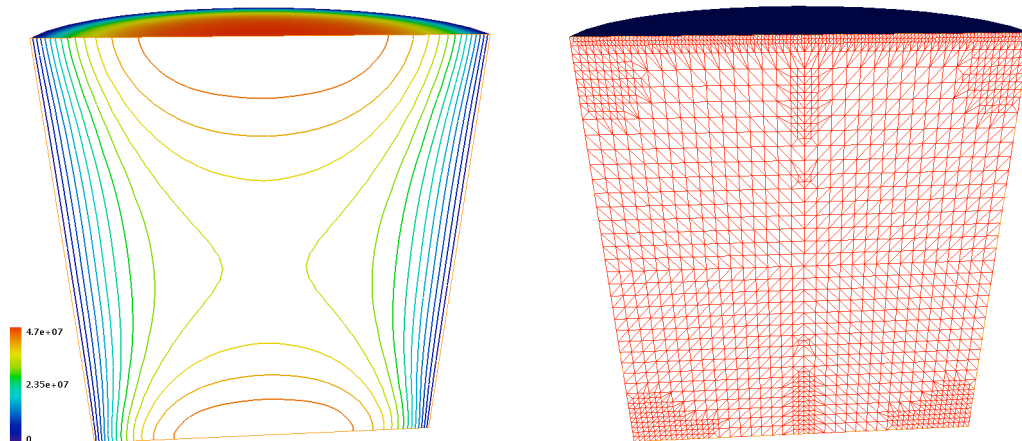
Figure 3: DPF for charcoal granite. Isolines of pore pressure at maximum of loading and corresponding adaptive mesh.

DPF: As initial time step $\delta t = 0.01$ is chosen. The adaptive mesh at final time $t = 1.0$ and the corresponding solution for the pore pressure on a section

plane is shown in Figure 3. The final time is reached after 3 time steps instead of 100 steps in case of absence of adaptive time control.

SBMF: Here, we solve the analogous problem using the SBMF equations for the trace of the stress tensor T and the pore pressure p. The displacement of the top face corresponds to increasing stress on top and bottom.
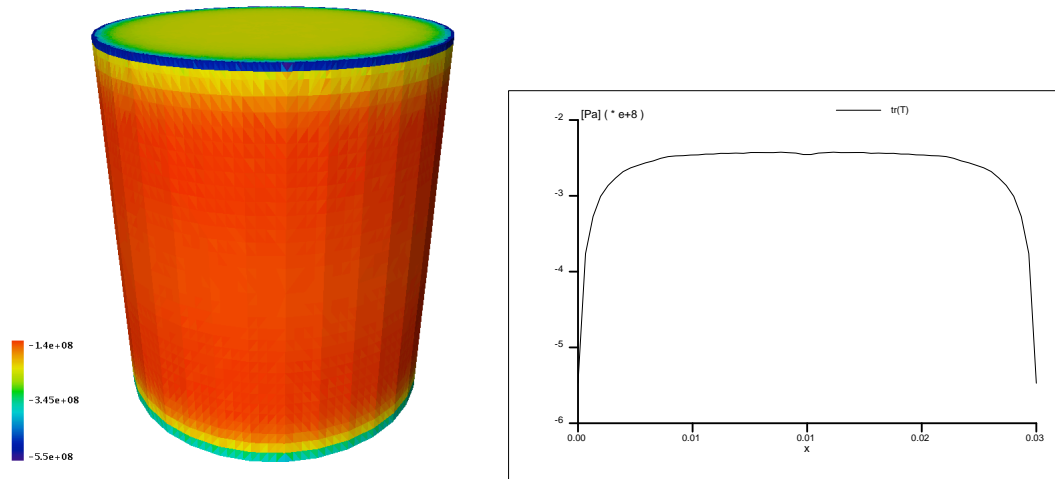

Figure 4: Charcoal granite. Trace of stress tensor T at time $t = 1$ on the boundary (left) and on a line through the top face (right).

For comparison with the DPF we take boundary values for stress as they resulted in the preceding calculation showing the typical singularities in the corners for the stress components. The profile of the trace of the stress tensor T at time $t = 1$ on the top face is presented in Figure 4. In our computation we scale the boundary values for the components of T linearly by the time t, $\quad 0 \leq t \leq 1$[sec]. In general it might be difficult to provide reasonable boundary conditions for the stress in the BMF or in the SBMF.

As initial time step $\delta t = 0.01$ is chosen. The final time is reached after only 3 adaptive time steps: $\delta t = 0.01$, 0.171, 0.819. That proves the efficiency of time control.

The adaptive mesh at time $t = 1.0$ and the corresponding solution for the pore pressure is shown in Figure 5. As expected the solution looks very similar to that of the DPF above. We get a good adaptation of the mesh close to the lateral boundary due to the steep gradient of the solution.

Figure 6 illustrates the change in pore pressure during one second of uniform increasing the loading on top and bottom.

All the linear algebraic systems in the finite element approximation are solved
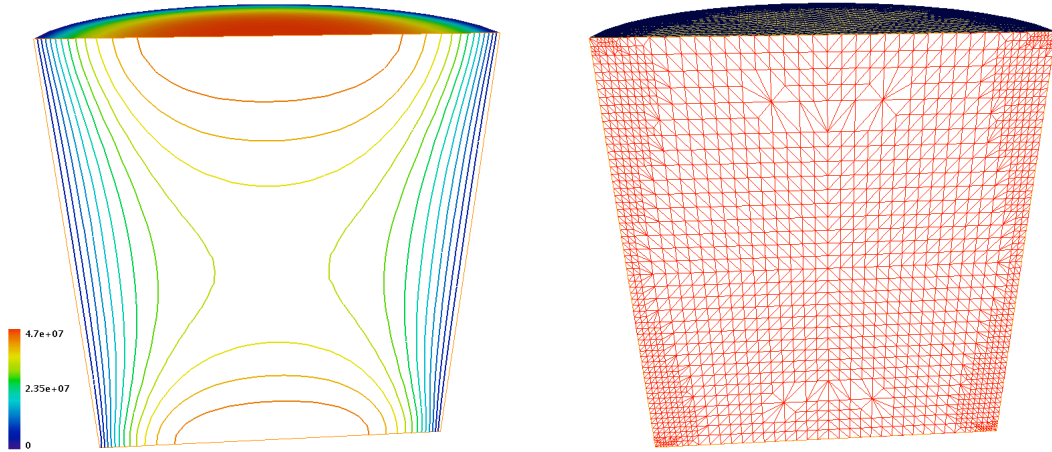
Figure 5: BMF for charcoal granite. Isolines of pore pressure at maximum of loading and corresponding adaptive mesh.
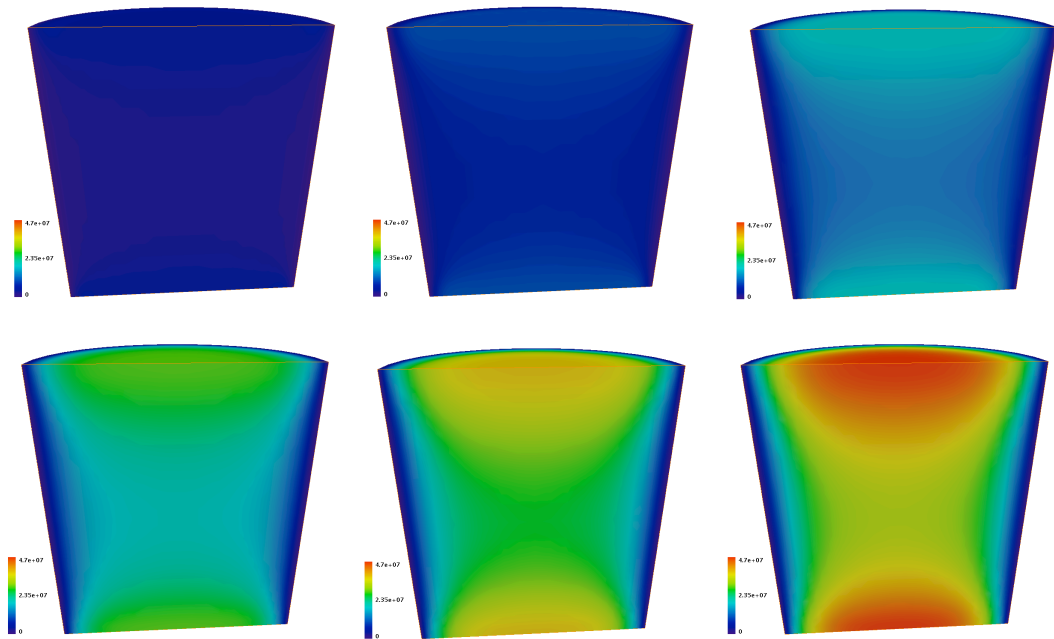

Figure 6: Charcoal granite. Development of pore pressure for time 0.1, 0.2, 0.4 (first row) and 0.6, 0.8, 1.0 sec (second row).

with the iterative solver which uses a moderate number of iterations, e.g., $100 - 260$ iterations for systems with about 430,000 unknowns or $400 - 450$

iterations for about 2,300,000 unknowns. A direct solver is not competitive for such systems.

4.2 Soft tissue

Next, we use the DPF for a simulation of soft material behavior based on the parameters of granulation tissue. However, the specific permeability $k = 1.0 \cdot 10^{-14}$ [m^2] is chosen larger by reason explained later.
We consider the loading case as described above and already studied for the charcoal granite, but this time we displace the top face 1 mm in direction of the bottom face which is fixed.
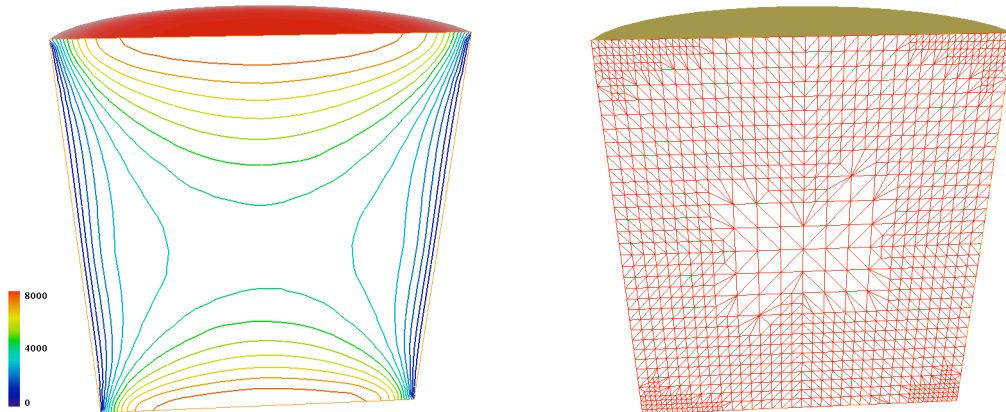
Figure 7: DPF for soft tissue. Isolines of pore pressure at maximum of loading and corresponding adaptive mesh.

As initial time step $\delta t = 0.025$ is chosen. The adaptive mesh at final time $t = 1.0$ and the corresponding solution for the pore pressure on a section plane is shown in Figure 7. The final time is reached after 5 time steps instead of 40 steps in case of absence of adaptive time control: $\delta t = 0.025$, 0.075, 0.184, 0.346, and 0.370.
Figure 8 illustrates the change of pore pressure during one second of uniform increasing the loading on top and bottom.
If we use initial time steps too small in this example, i.e., $\delta t \approx 0.005$, the solution of the linear system fails. Such phenomena are well-known in the context of algebraic-differential equations. They do not occur in the SBMF but therefor it is necessary to provide suitable profiles for the trace of the stress tensor on the boundary.
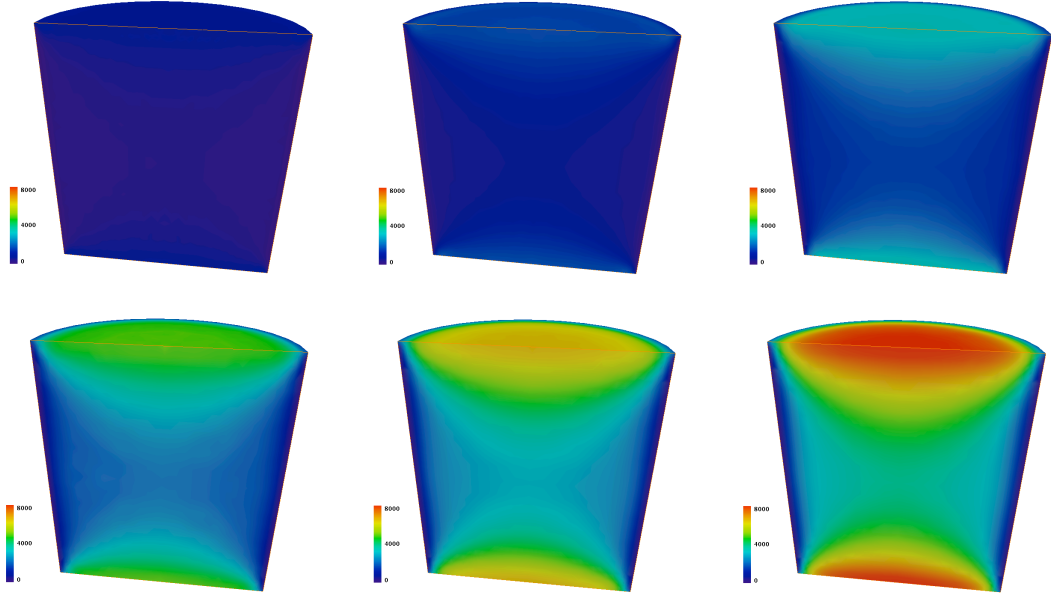
18

Figure 8: Soft tissue. Development of pore pressure for time 0.1, 0.2, 0.4 (first row) and 0.6, 0.8, 1.0 sec (second row).

4.3 Granulation tissue

Granulation tissue is also a soft tissue. It occurs for example in the gaps of bone fractures. It is defined by the parameters given in Table 2 which are the same as for the soft tissue we simulated in the section above, but the value for the specific permeability k is now reduced by factor 1000, i.e., $k = 1.0 \cdot 10^{-17}$ [m^2]. To get a good resolution of the solution in the 3D model the calculation would exceed the capacities of our computers. So, we utilize the axisymmetry of the problem and do the simulation in two space dimensions (2D).

Due to the axial symmetry of the cylinder we can easily transform the last 3D configuration to a 2D problem with coordinates r and z, see [41]. On the axis of symmetry, $r = 0$, we have the conditions $T^s n = 0$ and grad $p \cdot n = 0$. **DPF**: We start with the DPF assuming the same loading as in the study of soft tissue. Hence we have the same boundary conditions. Starting with $\delta_0 = 0.025$ as initial time step on a coarse initial grid (corresponding to the mesh in 3D) we reach the final time $t = 1.0$ by adaptive control already after 3 time steps: $\delta = 0.025, 0.206, 0.769$. Figure 9 shows the solution and the mesh for the final time. A more precise impression of the dynamics in the solution and the adaptive refinement is given by Figure 10 which is zoomed in
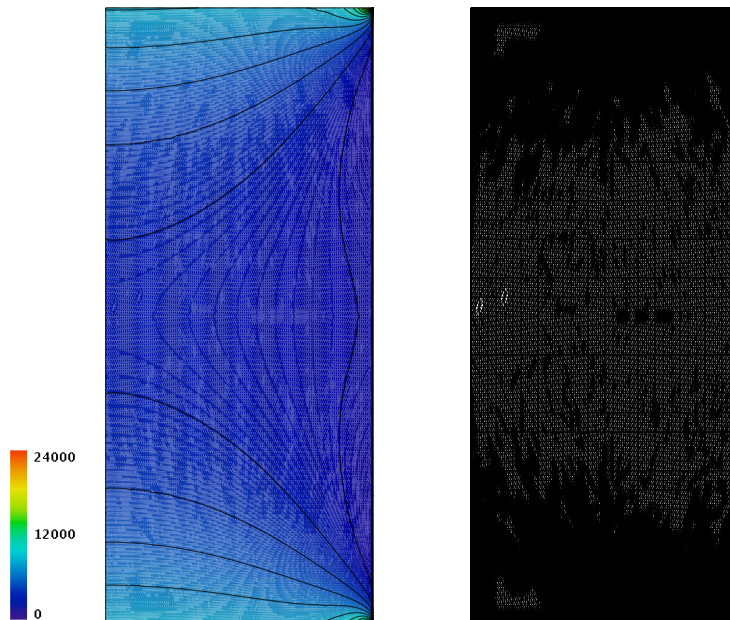
Figure 9: DPF for granulation tissue. Pore pressure at maximum of loading and corresponding adaptive mesh.

the upper right corner of the last figure. We recognize the correct adaptation of the mesh at the lateral boundaries and around the maximum of p due to the steep gradients. In particular it becomes clear why the analogous computation in 3D would take so much resources of memory.

Figure 11 shows the development of the solution for decreasing values of permeability, i.e., $k = 10^{-14}$, $k = 10^{-15}$, $k = 10^{-16}$, and $k = 10^{-17}$. It illustrates the more and more singular character of the solution and makes understandable the need of highly resolved meshes.

SBMF: Finally, we compute solutions of the model SBMF for the 2D simplification of the cylindrical geometry. As boundary condition for the trace of the stress tensor we use the results of the preceding calculation. For pore pressure we assume the same boundary condition as in the DPF.

The adaptive process starts on the same initial grid as in the calculation based on the DPF. The qualitative and quantitative behavior of the pressure is very similar to that in the DPF, compare the pore pressure p in Figure 12 and Figure 9. As expected there is a high agreement in the adaptive refined grids.

The calculation of the solution in the SBMF is much faster than the analogous calculation in the DPF because we have only two equations. However,
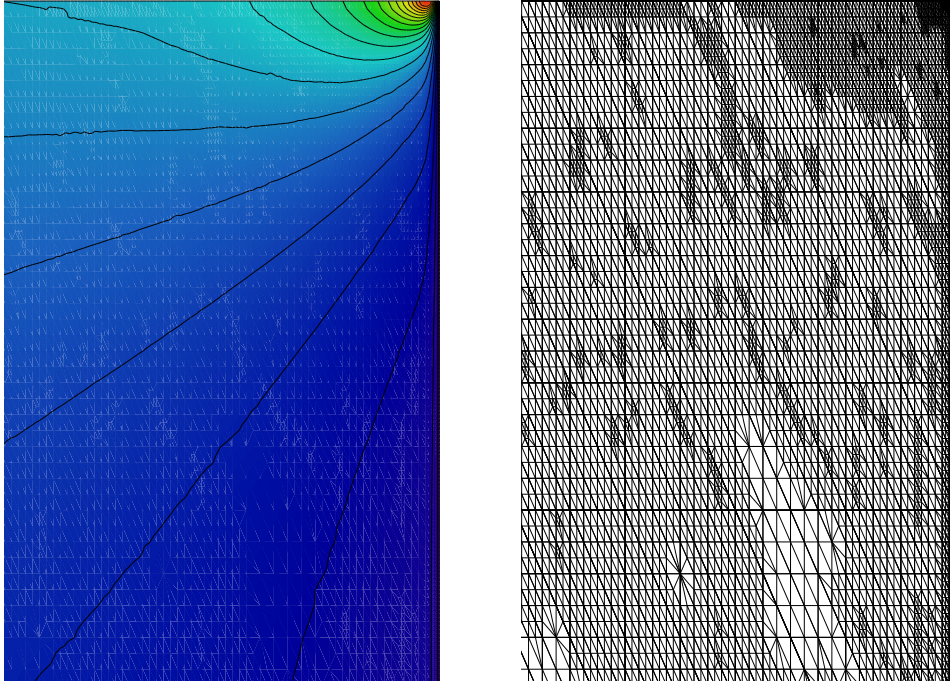
Figure 10: DPF for granulation tissue: Pore pressure at maximum of loading and corresponding adaptive mesh zoomed in the upper right corner of the region.
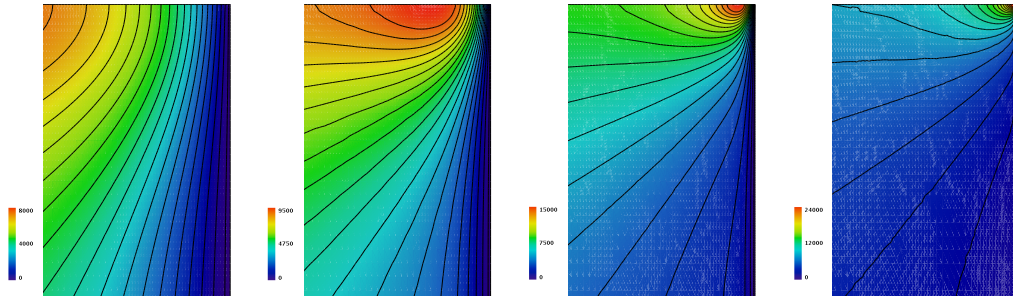

Figure 11: DPF for granulation tissue using different values for the specific permeability ($k = 10^{-14}$, $k = 10^{-15}$, $k = 10^{-16}$, and $k = 10^{-17}$). Pore pressure at maximum of loading in the upper right corner of the region.

we note again that in general it is not easy to find reasonable boundary conditions for the trace of the stress tensor.
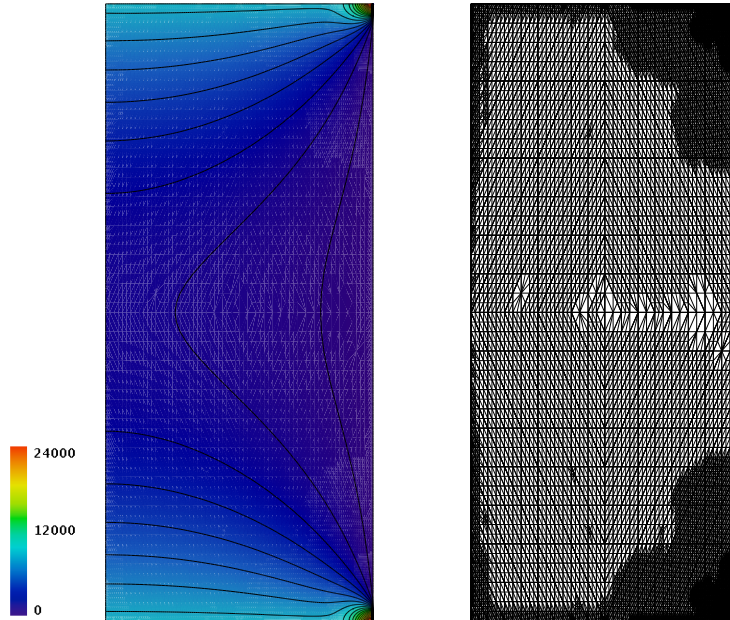
Figure 12: SBMF-model for granulation tissue. Pore pressure at time t = 1.0 and corresponding adaptive grid.

4.4 Bone

Bone is a stiff tissue. It is defined by the parameters given in Table 2. Simulations of the DPF in 3D would exceed our computational resources as in the case of granulation tissue. Therefore, we also restrict to the 2D calculation using the axisymmetry of the problem.

We assume the same loading as in the study of charcoal granite. Hence we have the same boundary conditions. We choose $t = 0.01$ as initial time step and reach the final time $t = 1.0$ by adaptive control already after 3 time steps: $\delta = 0.01, 0.95, 0.04$. Figure 13 shows the solution and the adaptive mesh for the final time. We prefer solving the linear algebraic systems in the FEM approximation by the direct method, because the iterative solver (GMRES preconditioned by ILU) takes too much iterations, e.g., 143 for a system with 2,232 unknowns, or 1,450 for 58,080 unknowns.

Here we abstain from presenting the corresponding results of the SBMF for bone. It provides the same results for the pore pressure if we invest the profile of the trace of the stress tensor resulting from the preceding calculation. In this model the iterative solver takes less iterations and becomes competitive, e.g., 20 iterations for a systems with 1,114 unknowns, or 160 iterations for 38,010 unknowns.
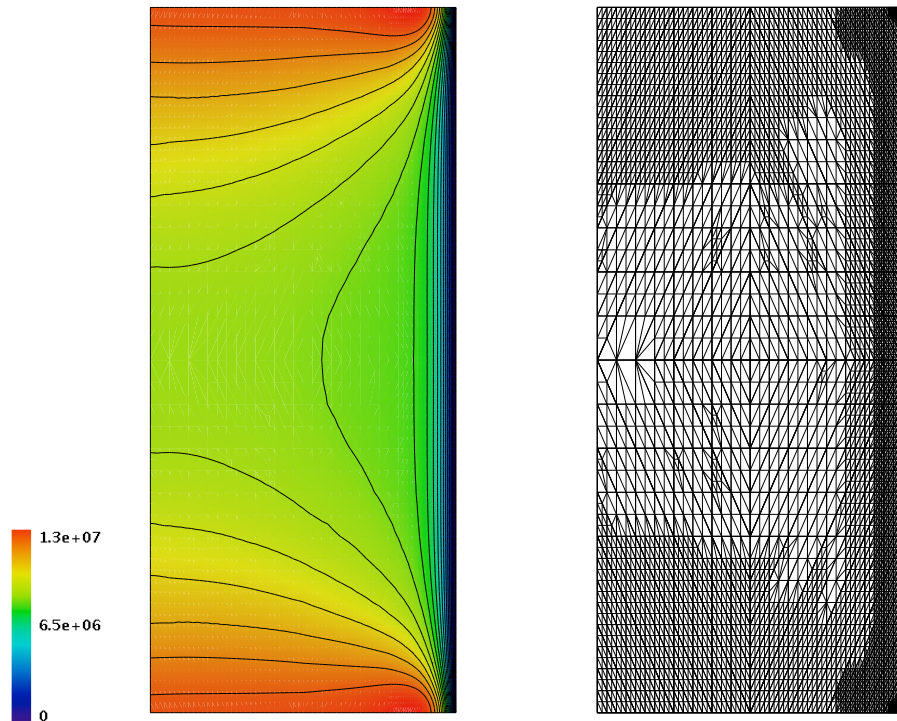
22

Figure 13: DPF for bone. Pore pressure at maximum of loading and corresponding adaptive mesh.

5 Conclusion and Outlook

In all our examples the adaptive mechanism of Kardos performed very well both for soft and stiff tissues. Hence, this method offers a way to find solutions efficiently in all cases where local dynamics occur in space or time. Especially, the control of time steps allowed to find the solution at final time by a small number of time steps. Both error estimation in time and space guarantee the reliability of the solution process.

Some disadvantage inherent the BELTRAMI-MICHELL description of linear poroelasticity is the difficulty of defining compatible boundary conditions. This problem does not occur in the *displacement-pressure* formulation (1) where the boundary conditions are canonically given by displacements. However, our code proved to be very efficient for the BELTRAMI-MICHELL model if the boundary conditions are known. This model might get more importance if it would be possible to provide a complete set of boundary conditions like in the complete BELTRAMI-MICHELL model for linear elasticity.

23

Solving the equations of the *displacement-pressure* model with our code, there occur problems in finding a solution for extreme values of the material parameters (as for granulation tissue or bone) or for too small time steps. Furthermore we observed a high number of iterations for solving the linear algebraic systems associated to the spatial discretization.

Future work will address these problems and try to extend the range of applications especially in three space dimensions.

6 Acknowledgement

References

[1] *http://amira.zib.de/*.

[2] *http://www.zib.de/Numerik/numsoft/kardos*.

[3] B. Albers, *Makroskopische Beschreibung von Adsorptions-Diffusions-Vorgängen in porösen Köpern*, PhD thesis, Techn. Univ. Berlin, 2000.

[4] R. Bank, *PLTMG: A Software Package for Solving Elliptic Partial Differential Equations - User's Guide 8.0*, SIAM, 1998.

[5] R. Bank and R. Smith, *A posteriori error estimates based on hierarchical bases*, SIAM J. Numer. Anal., 30 (1993), pp. 921–935.

[6] M. A. Biot, *Acoustics, Elasticity, and Thermodynamics of Porous Media: Twenty-one Papers by M.A. Biot*, Acoustical Society of America,, Woodbury, New York, 1992.

[7] F. Bornemann, *An adaptive multilevel approach to parabolic equations. III. 2d error estimation and multilevel preconditioning*, IMPACT of Comput. in Sci. and Engrg., 4 (1992).

[8] F. Bornemann, B. Erdmann, and R.Kornhuber, *A posteriori error estimates for elliptic problems in two and three space dimensions*, SIAM J. Numer. Anal., 33 (1996), pp. 1188–1204.

[9] H. Chen, R. Ewing, S. Lyons, G. Qin, T. Sun, and D.P.Yale, *A numerical algorithm for single phase fluid flow in elastic porous media*, Lecture Notes in Physics, 552 (2000), pp. 80 – 92.

[10] O. Coussy, *Poromechanics*, Wiley, 2003.

[11] S. Cowin, *Bone poroelasticity*, J. Biomech., 32 (1999), pp. 217–238.

[12] ——, *A recasting of anisotropic poroelasticity in matrices of tensor components*, Transport in Porous Media, 50 (2003), pp. 35–56.

[13] L. Cui, A. Cheng, V. Kaliakin, Y. Abousleiman, and J.-C. Roegiers, *Finite element analyses of anisotropic poroelasticity: A generalized Mandels's problem and an inclined borehole problem*, Int. J. Numer. Analyt. Meth. Geomechanics, 20 (1996), pp. 381–401.

[14] T. Davis, *Umfpack version 4.4*, 2005.

[15] K. Dekker and J. Verwer, *Stability of Runge-Kutta Methods for Stiff Nonlinear Differential Equations*, North-Holland Elsevier Science Publishers, 1984.

[16] P. Deuflhard, *Uniqueness theorems for stiff ode initial value problems*, in Numerical Analysis 1989, Proceedings of the 13th Dundee Conference, Pitman Research, D. Griffiths and G. Watson, eds., vol. 228 of Pitman Research Notes in Mathematics Series, Longman Scientific and Technical, 2000.

[17] P. Deuflhard, J. Lang, and U. Nowak, *Adaptive algorithms in dynamical process simulation*, in Progress in Industrial Mathematics at ECMI'94, H. Neunzert, ed., Wiley–Teubner, 1996, pp. 122–137.

[18] P. Deuflhard, P. Leinen, and H. Yserentant, *Concepts of an adaptive hierarchical finite element code*, IMPACT of Comput. in Sci. and Engrg., 1 (1989), pp. 3–35.

[19] B. Erdmann, J. Lang, and R. Roitzsch, *Kaskade manual, version 2.0*, Technical Report TR-93-5, Zuse Institute Berlin (ZIB), 1993.

[20] ——, *Kardos user's guide*, Technical Report ZR-02-42, Zuse Institute Berlin (ZIB), 2002.

[21] R. Ewing, O. Iliev, R. Lazarov, and A. Naumovich, *On convergence of certain finite difference discretizations for 1d porelasticity interface problems*, Tech. Rep. 69, Fraunhofer ITWM, 2004.

[22] F. Gaspar, F. Lisbona, C. Oosterlee, and R. Wienands, *A systematic comparison of coupled and distributive smoothing in multigrid for the poroelasticity system*, Numer. Linear Algebra Appl., 11 (2004), pp. 93 – 113.

[23] K. Gustafsson, *Control–theoretic techniques for stepsize selection in implicit Runge-Kutta methods*, ACM Trans. Math. Software, 20 (1994), pp. 496–517.

[24] K. Gustafsson, M. Lundh, and G. Söderlind, *A PI stepsize control for the numerical solution of ordinary differential equations*, BIT, 28 (1988), pp. 270–287.

[25] E. Hairer and G. Wanner, *Solving Ordinary Differential Equations II, Stiff and Differential-Algebraic Problems, Second Revised Edition*, Springer-Verlag, Berlin, Heidelberg, New York, 1996.

[26] D. Lacroix and P. Prendergast, *A mechano-regulation model for tissue differentiation during fracture healing: analysis of gap size and loading*, J. Biomech., 35 (2002), pp. 1163–1171.

[27] J. Lang, *Adaptive fem for reaction-diffusion equations*, Appl. Numer. Math., 26 (1998), pp. 105–116.

[28] ——, *Adaptive Multilevel Solution of Nonlinear Parabolic PDE Systems. Theory, Algorithm, and Applications.*, vol. 16 of LNCSE, Springer-Verlag, 2000.

[29] J. Lang and J. Verwer, *Ros3p - an accurate third-order Rosenbrock solver designed for parabolic problems*, BIT, 41 (2001), pp. 730–737.

[30] J. Lang and A. Walter, *A finite element method adaptive in space and time for nonlinear reaction–diffusion systems*, IMPACT of Comput. in Sci. and Engrg., 4 (1992), pp. 269–314.

[31] K. Lipnikov, *Numerical methods for the Biot model in poroelasticity*, PhD thesis, University of Houston, USA, 2002.

[32] C. Lubich and M. Roche, *Rosenbrock methods for differential-algebraic systems with solution-dependent singular matrix multiplying the derivative*, Comput., 43 (1990), pp. 325–342.

[33] S. Matera, *On reactive diffusive flows in porous media with regard to gasification of biomass*, Mitteilungen aus dem Rudolf-Drawe-Haus, TU Berlin, Inst. für Energietechnik EVUR, 2005.

[34] S. N. Patnaik and D. A. Hopkins, *Stress formulation in three-dimensional elasticity*, NASA Glenn Technical Reports Server, (2001).

[35] H. Rosenbrock, *Some general implicit processes for the numerical solution of differential equations*, Computer J., (1963), pp. 329–331.

[36] Y. Saad and M. Schultz, *GMRES: A generalized minimal residual algorithm for solving non-symmetric linear systems*, SIAM J. Sci. Stat. Comput., 7 (1986), pp. 856–869.

[37] D. Stalling, M. Westerhoff, and H.-C. Hege, *Amira: A highly interactive system for visual data analysis*, in The Visualization Handbook, C. Hansen and C. Johnson, eds., Elsevier, 2005, ch. 38, pp. 749–767.

[38] C. Truesdell, *Rational Thermodynamics*, Springer, 2nd ed., 1984.

[39] H. van der Vorst, *BI–CGSTAB: A fast and smoothly converging variant of BI–CG for the solution of nonsymmetric linear systems*, SIAM J. Sci. Stat., 13 (1992), pp. 631–644.

[40] J. Verwer, E. J. Spee, J. G. Blom, and W. Hundsdorfer, *A second-order Rosenbrock method applied to photochemical dispersion problems*, SIAM J. Sci. Comput., 20 (2002), pp. 1456–1480.

[41] H. F. Wang, *Theory of Linear Poroelasticity*, Princeton Series in Geophysics, Princeton University Press, 2000.

[42] K. Wilmański, *The thermodynamical model of compressible porous material with the balance equation of porosity*, Transport in Porous Media, 1 (1998), pp. 21–47.

[43] ——, *On themomdynamics of nonlinear poroelastic materials*, WIAS-Preprint, 792 (2002).

[44] ——, *On a micro-macro transition for poroelastic Biot's model and corresponding Gassmann-type relations*, WIAS-Preprint, 868 (2003).

[45] ——, *On Biot-like models and micro-macrotransitions for poroelastic materials*, WIAS-Preprint, 830 (2003).